Photocatalytic NOx abatement and self-cleaning performance of cementitious composites with g-C3N4 nanosheets under visible light

Yang, Yu; Ji, Tao; Su, Wenyue; Yang, Bin; Zhang, Yong; Yang, Zhengxian

DOI
10.1016/j.conbuildmat.2019.07.189

Publication date
2019

Document Version
Final published version

Published in
Construction and Building Materials

Construction and Building Materials 225 (2019) 120–131

Contents lists available at ScienceDirect

Construction and Building Materials

journal homepage: www.elsevier.com/locate/conbuildmat

Photocatalytic NO_x abatement and self-cleaning performance of cementitious composites with g-C_3N_4 nanosheets under visible light

Yu Yang [a,b], Tao Ji [b], Wenyue Su [c], Bin Yang [d], Yong Zhang [a,e], Zhengxian Yang [a,b,f,*]

[a] Fujian Provincial University Research Center for Advanced Civil Engineering Materials, Fuzhou University, Fuzhou 350116, China
[b] College of Civil Engineering, Fuzhou University, Fuzhou 350116, China
[c] State Key Laboratory of Photocatalysis on Energy and Environment, Fuzhou University, Fuzhou 350116, China
[d] Chengdu Design & Research Institute of Building Materials Industry Co., Ltd, Chengdu 610051, China
[e] Microlab, Section of Materials and Environment, Faculty of Civil Engineering and Geosciences, Delft University of Technology, Stevinweg 1, 2628 CN Delft, The Netherlands
[f] Department of Civil & Environmental Engineering, Washington State University, Pullman, WA 99164-2910, United States

HIGHLIGHTS

- The photocatalytic cement composites with g-C_3N_4 nanosheets (CNNs) were prepared.
- The CNNs based composites showed high visible light photocatalytic efficiency.
- The CNNs increased cement hydration degree leading a densified microstructure.
- The CNNs can improve the micro-hardness of the cementitious composites.

ARTICLE INFO

Article history:
Received 19 February 2019
Received in revised form 25 May 2019
Accepted 19 July 2019
Available online 23 July 2019

Keywords:
g-C_3N_4 nanosheets
Photocatalytic depollution performance
Self-cleaning
Cement hydration
Micro-hardness

ABSTRACT

The combination of photocatalyst with cementitious materials for air pollution abatement and self-cleaning has gained considerable attention. However, the most popularly used photocatalytic cementitious composites based on TiO_2 achieve the purification function under ultraviolet sunlight, significantly impeding a broader application of photocatalytic cementitious composites. Here, the photocatalytic cementitious composites were prepared by incorporating g-C_3N_4 nanosheets (CNNs) in Portland cement. With the increase of CNNs content, the photocatalytic NO_x abatement and self-cleaning performance was notably improved, while the micro-hardness of cementitious composites increased first and then decreased. Among the three mixing dosages (0.5%, 1% and 2% by weight of cement), the cementitious composite admixed with 2% CNNs showed the highest photocatalytic NO_x abatement efficiency of 227.3 $\mu mol\ m^{-2}\ h^{-1}$, and could degrade the rhodamine B within 40 min under visible light. Additionally, its microscopic hardness was 5.4% higher than the one without CNNs, suggesting that a moderate amount of CNNs (below 2%) in cementitious composites was effective in achieving an improved photocatalytic depollution performance.

1. Introduction

Air pollution is one of the major threats for the public health. Nitrogen oxides (NO_x) emitted from vehicle traffic and fossil fuel combustion is the main source for urban smog, depletion of tropospheric ozone and inception of acid rain, which would trigger serious respiratory, heart or lung diseases, and even premature death [1,2]. A promising solution lies in the utilization of semiconductor based photocatalysis driven by the inexhaustible and clean solar energy [3,4]. As illustrated in Fig. 1, by exposing the photocatalyst to solar light, the electrons (e^-) in the valence band are transferred to the conduction band leaving holes (h^+). The e^- and h^+ can reach the surface of the semiconductor particle initiating the redox process. The e^- of the conduction band with strong reducing potential reacts with oxygen to produce superoxide radicals ($\bullet O_2^-$). Then the $\bullet O_2^-$ reacts with water molecules to form the hydroxyl radicals ($\bullet OH$). On the other hand, the generated h^+ reacts with hydroxyl groups from water molecules, surrounding the photocatalyst, to form $\bullet OH$. Afterwards, the $\bullet OH$ acts as a strong oxidants with the potential to decompose a wide range of air pollutants (VOCs, NO_x, etc.) [5,6]. However, these semiconductors based photocatalysts are usually powdery. Therefore, in order to ensure its photocatalytic performance, nano-sized photocatalytic materials are

* Corresponding author at: College of Civil Engineering, Fuzhou University, Fuzhou 350116, China.
E-mail addresses: zhengxian.yang@wsu.edu, zxyang@fzu.edu.cn (Z. Yang).

https://doi.org/10.1016/j.conbuildmat.2019.07.189
0950-0618/

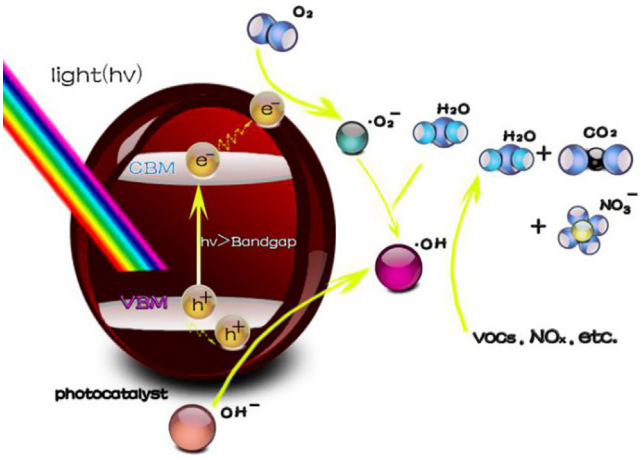

Fig. 1. Schematic illustration of the mechanism for photodegradation of the air pollutants.

often immobilized onto a supporting material or substrate to prevent loss from mechanical abrasion and environmental damages.

Due to the inherent porous feature, cementitious materials are the most potential substrate for the application of photocatalytic materials in building and construction industries. The surfaces of urban construction are typically exposed to the highest levels of air pollution. It is promising to apply photocatalysis on building materials as an attractive sustainable strategy to purify air pollutants and endow the building with self-cleaning and antimicrobial properties [7,8]. In this respect, the photocatalytic cementitious materials have been fabricated using various preparation methods, such as spray coating and intermixing. Martinez et al. applied a polymer-matrix-based coating incorporating nano-TiO_2 to the different substrates and found that the use of mortar as the substrate showed the best photocatalytic performance of degradation of NO [9]. Ângelo et al. reported a highly active photocatalytic paint incorporated with TiO_2 for outdoor NO_x abatement [10]. Guo et al. studied a TiO_2-intermixed concrete surface layer with good photocatalytic NO removal ability and found that harsh abrasion exerted no obvious deterioration to photocatalytic performance of TiO_2-intermixed cementitious materials [11]. The photocatalytic coatings on building materials often exhibits a weak adhesion to the substrates, rendering poor durability in aggressive outdoor environments [12]. In contrast, intermixing photocatalyst with cementitious materials is regarded as a facile and universal method to prepare photocatalytic cementitious composites, which harboured robust resistance to abrasion action and weathering in real-life service [11].

At present, titanium dioxide (TiO_2) is the most commonly used photo-catalyst because of its chemical stability and high reactivity. Thanks to its inert nature and ease of use, TiO_2 has been widely incorporated in building materials to improve the aesthetics and hygiene of urban infrastructures and to combat the urban air pollution [13,14]. However, due to its wide band gap (3.2 eV), TiO_2 can only be excited under UV irradiation to form photogenerated electron–hole pairs. It is unfortunate that only about 4.5% of the solar spectrum falls in the UV range [15]. This adversely impedes a broader application of TiO_2. Moreover, TiO_2 was recently reported for the possibility of causing cancer when inhaled [1]. Therefore, the development of nontoxic photocatalysts with an outstanding visible light activity that can be used in building materials is imperative.

Graphitic carbon nitride (g-C_3N_4), a typical graphite-like layered material, is well known as a nontoxic metal-free semiconductor [16]. With its unique features such as high thermal and chemical stability, high-hardness and visible-light driven band gap, g-C_3N_4 is considered as a kind of prospective photocatalyst in various applications including water splitting [17], CO_2 reduction [18], and pollutants removal [19,20]. Over the past few years, g-C_3N_4 has become a fascinating visible light driven photocatalyst for environmental pollution mitigation. Chang et al. found that the porous g-C_3N_4 prepared by a facile pyrolysis method showed remarkably photocatalytic performance in degradation of Rhodamine B (RhB) under visible-light [21]. Papailias et al. reported that the g-C_3N_4 obtained via thermal polycondensation of melamine could effectively remove NO_x under visible light [22]. Sano et al. found that the photocatalytic NO abatement of g-C_3N_4 under visible light could be significantly improved by 8.6 times compared to the conventional g-C_3N_4 via an alkaline hydrothermal treatment [23]. Compared to inherent wide band gap of TiO_2 (3.2 eV) which is excited only under UV irradiation, g-C_3N_4, owing to its narrow band gap of 2.7 eV, offers a great potential for air purification under visible light. Furthermore, g-C_3N_4 can be facilely synthesized in a large scale with low cost by polycondensation of various carbon and nitrogen-containing organic precursors.

Normally, there are two types of g-C_3N_4: bulk g-C_3N_4 and g-C_3N_4 nanosheets (CNNs). Compared with the bulk g-C_3N_4 prepared by traditional thermal polymerization, ultrathin CNNs are extremely advantageous for promoting photocatalysis efficiency. The apparent advantages associated with nanosheets include large specific surface area for providing abundant reactive sites and short bulk diffusion length for reducing the recombination probability of photoexcited charge carriers [24,25]. Recently, Kou and co-workers reported a new g-C_3N_4 based photocatalytic cement, showing an enhanced visible-light photocatalytic activity via construction of the SnO_2/g-C_3N_4 heterostructures to enhance electron-hole separation and interfacial charge transfer [26]. While limited research regarding the cementitious materials incorporated with CNNs for air purification and self-cleaning applications has been reported.

In this study, we introduce a novel photocatalytic cementitious composite based on CNNs. The photocatalytic performances in terms of NO_x removal in a continuous mode and discoloration of RhB were examined under visible light. Furthermore, the effect of CNNs on microscopic mechanical property of the cementitious materials, cement hydration and composite hydration products were investigated by micro-hardness, isothermal calorimetry, X-ray diffraction (XRD), Fourier transform infrared (FTIR), thermogravimetry (TG) and field emission scanning electron microscopy (FESEM). The primary objective of this study is therefore to provide a theoretical basis for the beneficial use of an earth-abundant g-C_3N_4 photocatalyst as a multifunctional material in sustainable building and constructions for improved environmental pollution mitigation.

2. Experimental

2.1. Materials

A grade 42.5R Portland cement which is in accordance with Chinese standard (GB/T17671-1999) was used. The composition of the cement in wt% is as follows: C_3S (tricalcium silicate): 55.6, C_2S (dicalcium silicate): 19.6, C_3A (tricalcium aluminate): 7.5, SO_3 (sulphur trioxide): 2.1, C_4AF (tetracalcium alumino ferrite): 9.3. Melamine, ammonium chloride and commercial titanium dioxide (TiO_2) were purchased from Sinopharm Chemical Reagent Co. Ltd. and used without further purification. Deionized water was used in all experiments.

2.2. The synthesis of g-C_3N_4 nanosheets

Motivated by a previous report [27] and thanks to the gases (NH_3 and HCl) released from NH_4Cl with the increase of tempera-

ture, the large-quantity and high-quality few-layer g-C_3N_4 nanosheets (CNNs) were prepared through a facile one step method. In a typical procedure, 4 g of melamine powders and 20 g ammonium chloride were fully mixed and heated at 550 °C for 4 h with a heating rate of 3 °C min^{-1}. Upon cooling down, the resultant fluffy agglomerates were milled into powders in an agate mortar for further use. The structural features of the as-prepared CNNs were investigated using XRD and FTIR (Fig. 2). Fig. 3 (a) shows the morphology of the CNNs, and the ultrathin thickness (approximately 5 nm) was further verified by AFM image (Fig. 3 (b) and (c)). The particle size distribution and nitrogen adsorption–desorption isotherms of the CNNs are shown in Fig. 4 and Fig. 5, respectively. Besides, the BET surface area of the CNNs is about 76.6 m^2 g^{-1}.

2.3. The preparation of photocatalytic cementitious composites

For the preparation of photocatalytic cementitious composites, the water/cement ratio for all batches was kept consistent at 0.4. The CNNs suspensions were firstly prepared by dispersing the CNNs (0.5, 1 and 2% by the weight of cement) into deionized water for 2 h under ultrasonication. Then ordinary Portland cement and CNNs suspension were mixed in a standard lab mixer for 2 min with a revolution speed of 200 ± 5 r min^{-1}, and another 2 min of 300 ± 5 r min^{-1}. After mixing, the fresh cementitious composites were cast into molds (diameter 30 mm, thickness 5 mm) under compaction on a vibration table. The samples were then left in the mould for 24 h before demoulding and cured in an environmental chamber at 20 ± 2 °C and over 95% relative humidity for 6 additional days before subjecting to assigned tests. As a preliminary exploration of using CNNs in cementitious composites, the effect of CNNs on cement hydration after 7 days was studied, as a representative. According to previous reports, the compressive strength and the hydration degree of 42.5R Portland cement cementitious composites cured for 7 days can reach 80–95% [28–30] and 75–91% [31], respectively, of that for 28 days, suggesting that the composites have reached a high maturity at a curing age of 7 days. In addition, the 2% TiO_2 added cement composite was prepared as reference sample in test of photocatalytic activity via the foregoing method.

2.4. Microscopic hardness

Microscopic hardness is a fast way for measuring the effects of CNNs on the mechanical properties of cementitious composites since it is directly related to the strength of a material [32]. Micro-hardness (HV) of photocatalytic cementitious composites were determined by a Vickers Microhardness tester (THVS-1-800M-AXY) with a load of 0.5 N. The sample was ground on an automatic machine using various sand paper with grade of #320, #600, #800, and #1200 sequentially, until a flat mirror surface was obtained. Then the ground sample was cleaned with deionized water and dried in a vacuum oven at 45 °C for 12 h. Statistical tests were carried out over each sample to ensure a reliable measurement of the local mechanical properties. The indentation was repeated for 30 times on different areas of the sample surface. The interval distance of adjacent vertexes was set as 50 μm.

2.5. Characterization

The phase compositions of samples were characterized by X-ray diffraction (XRD) analysis on a Bruker D8 Advance X-ray diffractometer with a Cu Kα ray source. Fourier transform infrared (FTIR) spectra were obtained using a Thermo Scientific Nicolet IS50 Fourier transform infrared spectrometer at a resolution of 2 cm^{-1}. A total of 64 scans were performed to obtain each spectrum. Thermogravimetry (TG) of samples was performed using a Netzsch STA449 F3 simultaneous Thermogravimetric analyser to measure the content of non-evaporable water (NEW) and hydration products in cementitious composites. The non-evaporable water (NEW) content measurement is one of the most intensively used methods of monitoring the degree of cement hydration [33]. The condition of TG analysis was in a nitrogen atmosphere (flow rate of 80 mL min^{-1}) at a heating rate of 10 °C min^{-1} up to 1000 °C. The morphology of the materials was observed by a Thermoscientific Verios G4 UC field emission scanning electron microscope (FESEM). A tapping-mode atomic force microscopy (AFM, Dimension Icon, Bruker) with Si-tip cantilever was used to probe the thickness of the synthesized CNNs on the mica substrate. The hydration heat of cementitious composites was measured by a TAM air isothermal microcalorimeter (TA Instruments, USA). The measurement of hydration heat was performed at an isothermal condition (25 ± 0.1 °C). The 5 g of Portland cement was firstly put into a sample ampoule of thermometric TAM. The as-prepared CNNs suspension was added to the sample ampoule with a syringe. Afterwards, the paste was mixed with a special electric stirrer for 90 s and placed into the chamber of TAM Air. The hydration heat evolution rate and cumulative hydration heat of the cementitious composites containing CNNs can be monitored as a function of time. The

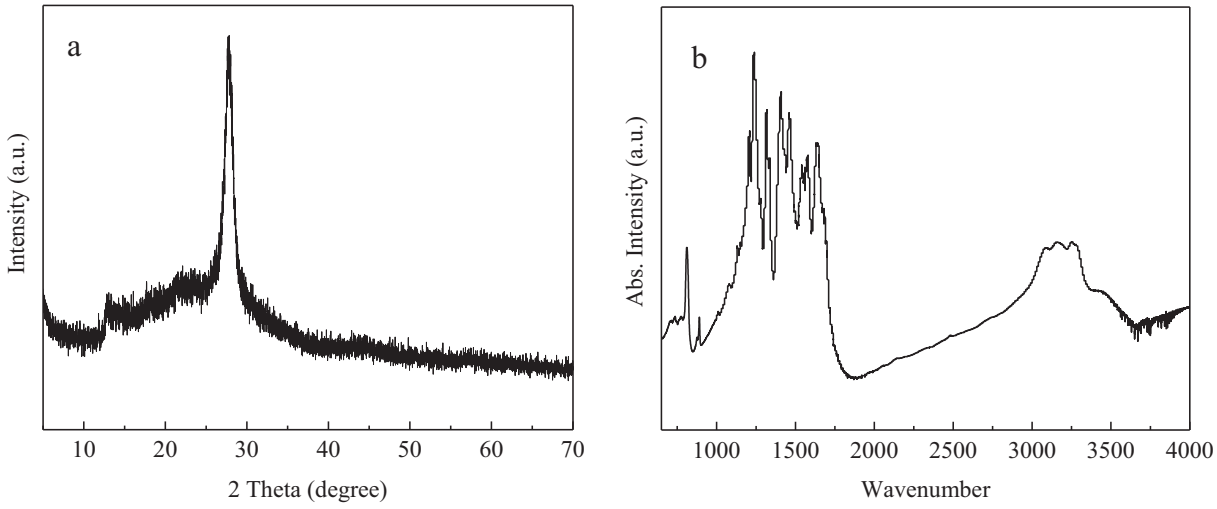

Fig. 2. (a) XRD patterns and (b) FTIR spectroscopy of CNNs.

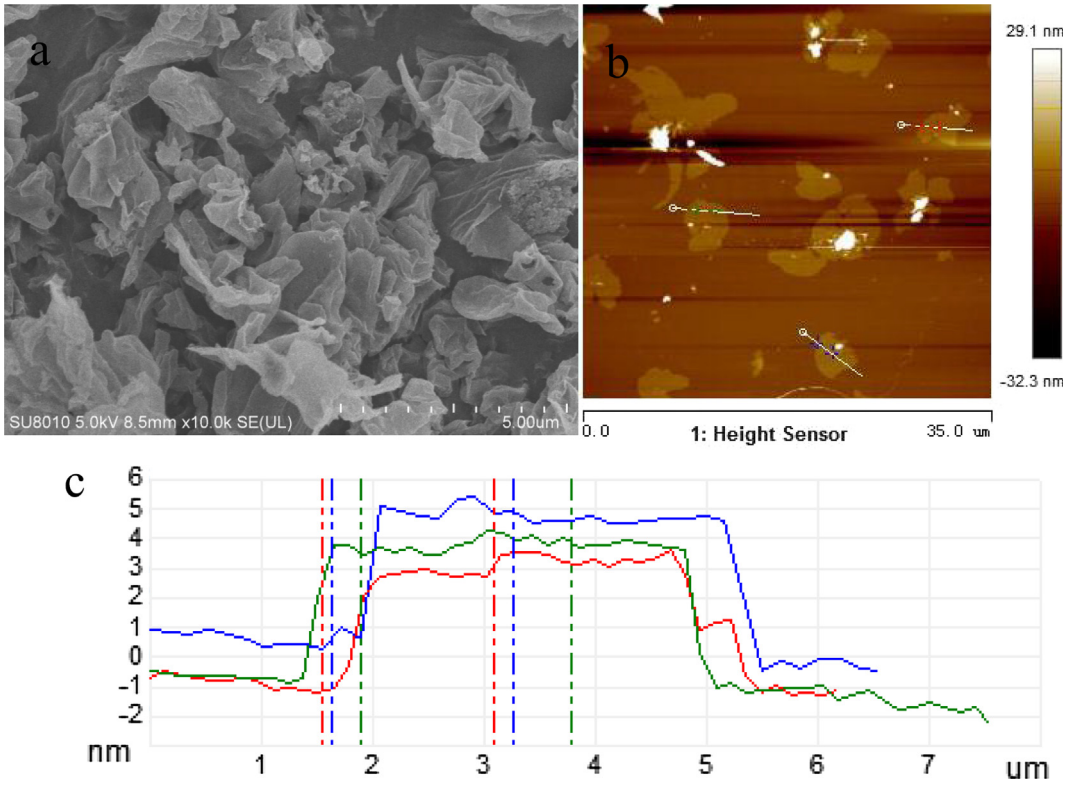

Fig. 3. (a) FESEM image, (b) AFM image and (c) corresponding cross-sectional profile of CNNs.

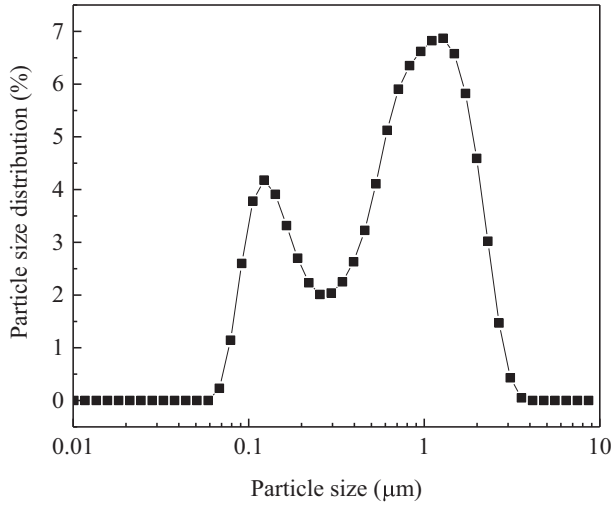

Fig. 4. Particle size distribution of CNNs.

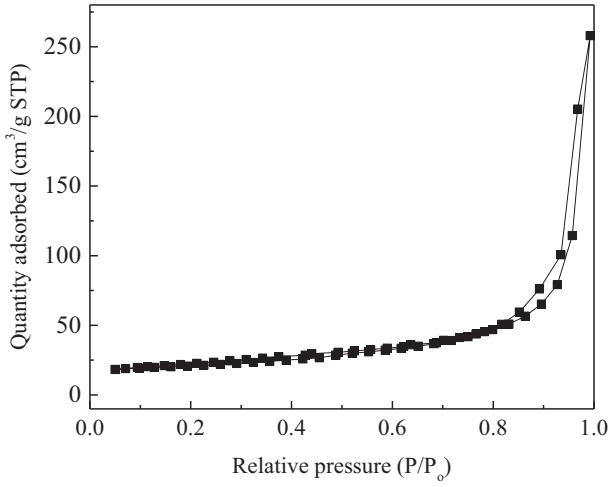

Fig. 5. Nitrogen adsorption–desorption isotherms of CNNs.

water/cement ratio (0.4) used was the same as to prepare the photocatalytic cementitious composites mentioned above.

2.6. Visible light photocatalytic activity

2.6.1. Visible light photocatalytic removal of NO_x in air

All the tests were carried out at ambient temperature (25 ± 2 °C). The photocatalytic NO_x abatement of the sample was evaluated by a continuous flow reactor adapted from an existing design[34] as illustrated in Fig. 6 (a). The volume of the cylindrical reactor, which was made of glass and covered with quartz glass window, was 141.3 mL (Φ60 mm × 50 mm) (Fig. 6(b)). One sample was placed in the middle of the reactor, and a 300 W xenon lamp with a light passed through a UV cut off filter (λ > 420 nm) was vertically placed outside the reactor as a light source. The required light intensity of 30 mW cm^{-2} on the surface of the samples was obtained by adjusting the distance between the lamp and the reactor. The initial concentration (1 ppm NO) of the testing gas was achieved with two mass flow controllers supply. The relative humidity of the testing gas was control at 50 ± 2% by the gas washing bottle before the gas entered the glass reaction chamber. The flow rate of the testing gas through the reactor was controlled at 1 L min^{-1} by a mass flow controller. Once the adsorption–desorption equilibrium reached, the lamp was turned on. The concentrations of NO and produced NO_2 were continuously measured using a NO_x analyzer (Model 42i, Thermo Environmental Instruments Inc). The removal amount of NO_x was calculated as following:

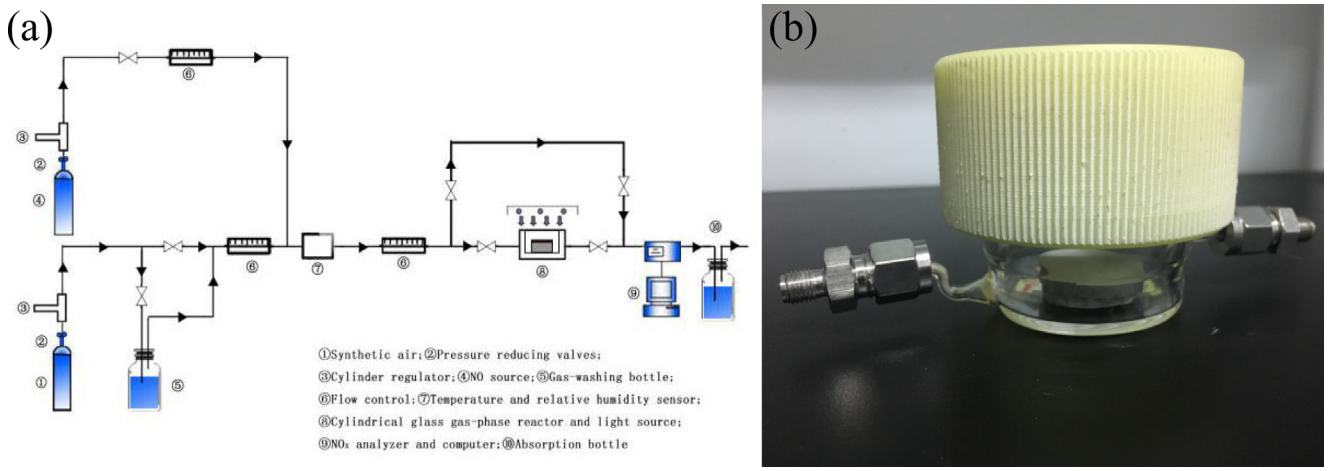

Fig. 6. (a) Schematic diagram of gaseous NO_x removal experimental set-up; (b) image of the reactor.

$$Q_{NOx} = \left(\frac{f}{22.4}\right)\left\{\int ([NO]_0 - [NO])dt - \int ([NO_2] - [NO_2]_0)dt\right\}/(A \times T) \quad (1)$$

where Q_{NO_x} (μmol m^{-2} h^{-1}) is the amount of nitric oxides removed by the test sample; $[NO]_0$ and $[NO_2]_0$ (ppm) are t is the initial concentration of nitrogen monoxide and nitrogen dioxide respectively without visible light; [NO] and $[NO_2]$ (ppm) are the outlet concentration of nitrogen monoxide and nitrogen dioxide respectively under visible light irradiation; t (min) is the time of removal operation; f (L min^{-1}) is the flow rate at the standard state (273 K, 1.013 kPa); A (m^2) is the surface area of cement composite samples; T (30 min for all experiments) is the duration of the photocatalytic process, and 22.4 represents that the volume of 1 mol ideal gas at the standard state is 22.4 L (ideal gas law).

2.6.2. Self-cleaning test

The self-cleaning performance of the sample was evaluated following a procedure reported elsewhere [35]. Typically, a plastic ring (diameter 2.0 cm) was glued on the surface of as-prepared photocatalytic cementitious composites. 1 mL rhodamine B (RhB) solution with a concentration of 1.0 mmol L^{-1} was applied evenly on the surface of samples within the plastic ring. Then the specimens were oven dried at a temperature of 40 °C for 10 h. After drying, one sample was placed horizontally under a 300 W xenon lamp with a light passed through a UV cutoff filter (λ > 420 nm). The required light intensity of 30 mW cm^{-2} on the surface of the samples was obtained by adjusting the distance between the lamp and the samples. To avoid temperature rise, the samples were cooled down using an electrical fan during the operation. The color change of the dye applied on the photocatalytic specimens which were subjected to different light irradiation time (i.e., 0, 10, 20, 30, 40, 50 and 60 min in this study) were pictured by a Nikon D7000 SLR camera (the distance between the camera lens and the specimen remained the same 10 cm). The histogram analysis of the obtained images was analyzed by the software ImageJ64 1.35.

The removal efficiency of RhB was evaluated as follows:

$$\delta\% = \frac{C_0 - C_t}{C_0} \times 100\% \quad (2)$$

where C_0 and C_t are the concentration of the initial and remaining RhB respectively; t is the light illumination time.

3. Results and discussion

3.1. The effect of CNNs on early microscopic mechanical property of cementitious composites

The microscopic hardness of cementitious composites containing different dosages of CNNs (0, 0.5, 1, 2% by weight of cement) which were cured for 7 days is displayed in Fig. 7. With the addition of CNNs, a parabolic growth tendency of the microscopic hardness of cementitious composites can be observed. The microscopic hardness of the cementitious composites with 2, 1 and 0.5% CNNs are 105.4, 115.3 and 117.9% respectively of the one without CNNs due to the strengthening effect of CNNs. When the CNNs content is >0.5%, the microscopic hardness tends to slightly decrease, which can be attributed to the increased probability of agglomeration of CNNs in cementitious composites. This phenomenon agrees with a previous study that the cluster of the nano-materials weakened the microscopic hardness of cementitious composites [36]. Additionally, due to the high specific area, the addition of CNNs often leads to the increasing in the water demand, resulting in an increase in porosity [37]. This can also be responsible for the decline in microscopic hardness.

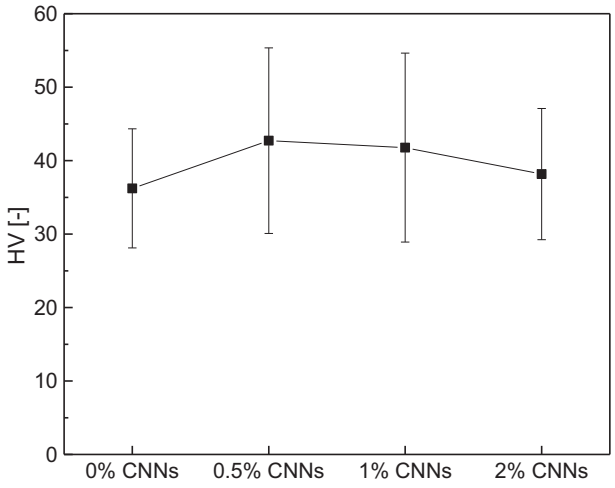

Fig. 7. Microscopic hardness of cementitious composites with different content of CNNs.

3.2. The effect of CNNs on early hydration of cement

The hydration process of cementitious composites containing CNNs was monitored by isothermal calorimetry (TAM Air). Fig. 8 (a) shows the heat flow curves of the cementitious composites containing different dosages of CNNs. It is well known that cement hydration is a dissolution-precipitation process [38] and all specimens display two significant heat flow maxima during the main period. As can be seen in Fig. 8(a), the first peak of the samples containing CNNs starts earlier than that of the samples without CNNs. The addition of the CNNs greatly increases the intensity of the first heat peak, especially for the 2% addition. All the samples containing CNNs show a slightly higher intensity of the second heat evolution peak in comparison with the reference sample. Fig. 8(b) shows the curves of the cumulative heat evolution during the first 100 h hydration. The increasing cumulative heat release at 2 h hydration can be observed with addition of CNNs, consistent with the heat evolution rate during the first heat peak. This indicates that the addition of CNNs can significantly accelerate the early hydration of cement, mainly resulting from the aluminate reaction [39]. The heat evolution of the second heat peak during the 2–100 h hydration can be attributed to the silicate reaction, C_3A dissolution and ettringite precipitation [40]. With the increasing time of hydration up to 100 h, although there is no significant difference of the cumulative heat, the samples containing 0.5 and 1% CNNs show a slight increase in the cumulative heat evolution with respect to that of pure cementitious composites, indicating an enhanced degree of hydration due to a multiplication of heterogeneous nucleation sites provided by CNNs. It is also widely accepted that the ultra-fine particles could act as potential heterogeneous nucleation sites for the hydration products, resulting in an acceleration of cement hydration [41,42]. However, too much CNNs would obstruct the contact between cement particles and water, which is a disadvantage for the hydration process of cement. This results in a lower cumulative heat evolution at 100 h hydration for the 2% CNNs-added cementitious composites.

In order to investigate the effect of CNNs on the hydration crystals of cementitious composites, XRD patterns of CNNs-added cementitious composites hydrated for 7 days were investigated. As shown in Fig. 9 (a), although the characteristic peaks of the CNNs were not found in the XRD patterns due to its tiny amounts in the composites or its inherent low crystallinity, the peaks of calcium hydroxide (CH) and calcite were detected clearly for all samples while no other new phases were observed with increasing CNNs dosage. On the other hand, differences were found in the relative intensities of the (0 0 1) and (1 0 1) peaks of CH for all the samples, indicating the different preferential orientation growth of CH under conditions with different CNNs dosages. It can be observed in Fig. 9 (b) that the relative intensities of the (0 0 1) and (1 0 1) peaks decrease gradually with increasing CNNs dosage, suggesting that the CNNs lowered the orientation index of CH crystals, which can be attributed to the nucleation effect of CNNs. And

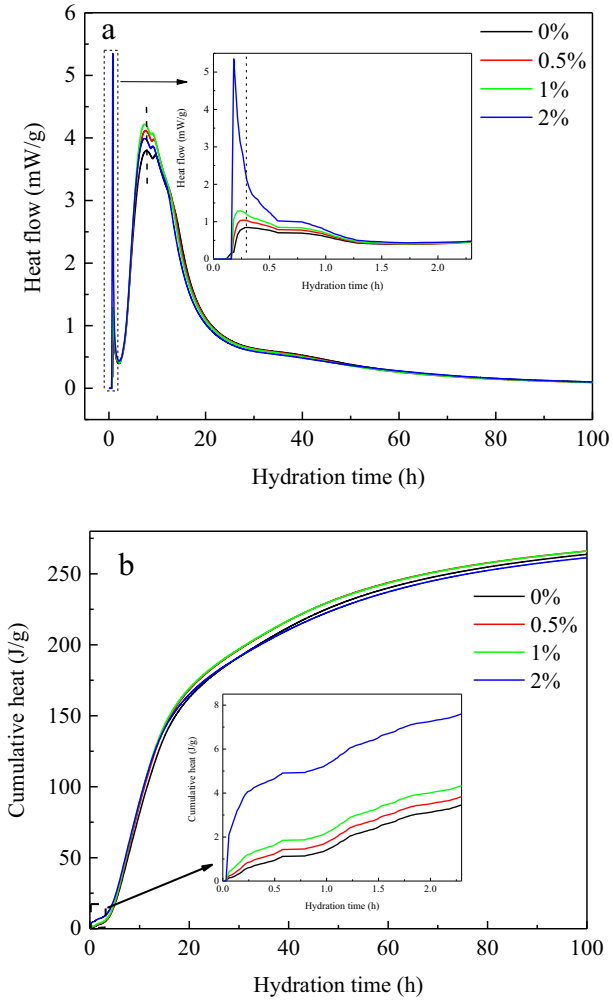

Fig. 8. (a) Heat flow curves and (b) Cumulative hydration heat for cementitious composites with different content of CNNs.

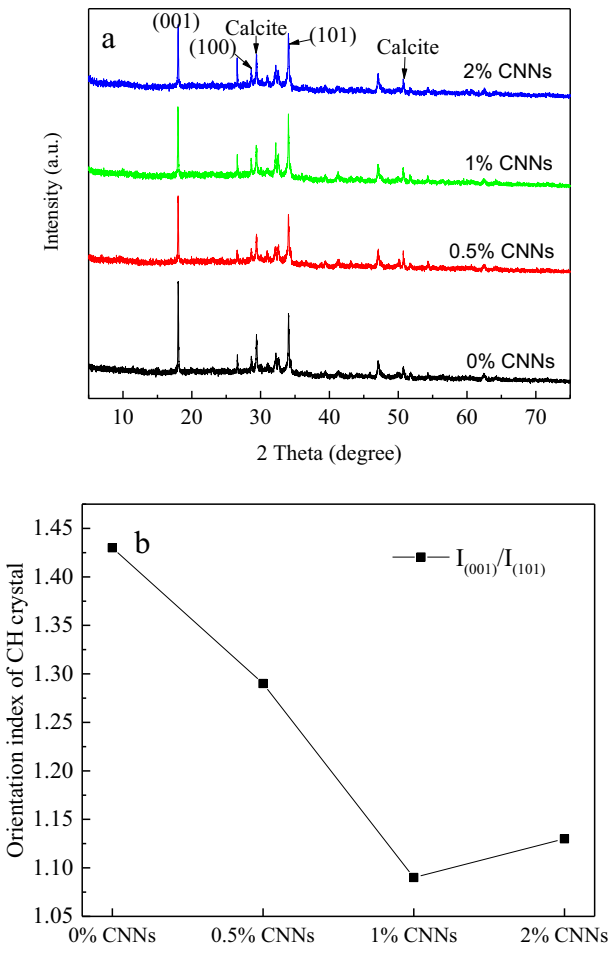

Fig. 9. (a) XRD patterns and (b) orientation index of CH crystal of cementitious composites with different content of CNNs.

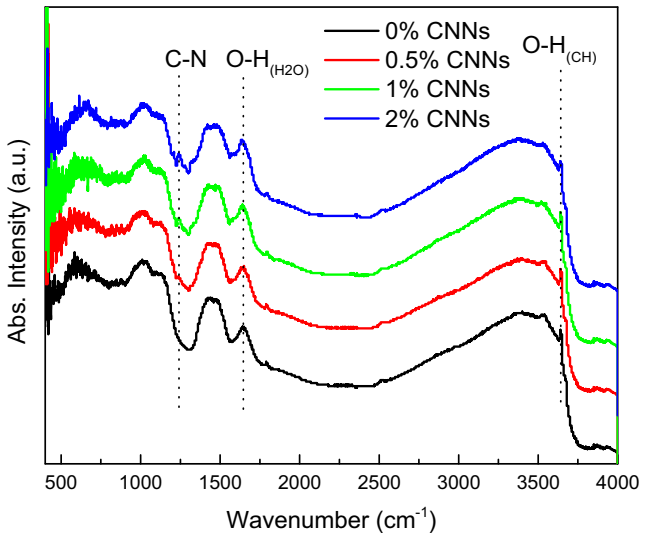

Fig. 10. FTIR spectroscopy of cementitious composites with different content of CNNs.

the diminished orientation of CH crystals has been reported to be able to improve the interface structure of cementitious composites [43,44].

Fig. 10 represents FTIR patterns of cementitious composites with different contents of CNNs hydrated for 7 days. After the introduction of the increased content of CNNs, the growing peak at 1250 cm^{-1} originated from tri-s-triazine heterocyclic rings in CNNs is observed clearly, suggesting that the composite materials were successfully prepared. The band appeared at 1650 cm^{-1} is attributed to the stretching and bending vibration of the chemically bound water in the calcium silicate hydrate (C-S-H) [45,46]. A slightly negative shift of the peak at 1650 cm^{-1} with the addition of CNNs was observed indicating the formation of strong bond between C-S-H and CNNs. The interaction between the CNNs and the cement hydrates can improve the load-transfer efficiency from the cementitious composites to CNNs. Consequently, the microscopic hardness of the cementitious composite was enhanced. The peak at 3640 cm^{-1} is attributed to the O–H of portlandite phase [47]. For the 0.5 and 1% CNNs-added cementitious composites, the intensity of the O–H group of CH increase slightly compared to that of pure cementitious composite while the 2% CNNs-added cement composite shows a declined intensity. This suggested that the addition of 0.5 and 1% of CNNs help increase the content of CH in cementitious composites while the addition of 2% CNNs exerted a negative impact on the formation of portlandite.

Fig. 11 shows the TG/DTG curve of cementitious composites with different CNNs dosages hydrated for 7 days. There are 3 endothermic peaks in the DTA curves attributed to the decomposition of C-S-H [48], CH [49] and calcite [50] respectively, which is in good agreement with the mineralogical characterization in XRD analysis (Fig. 9(a)). The content of non-evaporable water (NEW) is measured as the weight loss of the sample between 105 °C and 1000 °C [43]. Using formula (3), the NEW at different CNNs contents was calculated and shown in Fig. 12.

$$NEW = W_{105^{\circ}C} - W_{1000^{\circ}C} - W_{CaCO_3} - W_{CNNs} \quad (3)$$

where NEW is the weight percentage of non-evaporable water; $W_{105^{\circ}C}$ is the percentage of weight loss after 105 °C heat treatment;

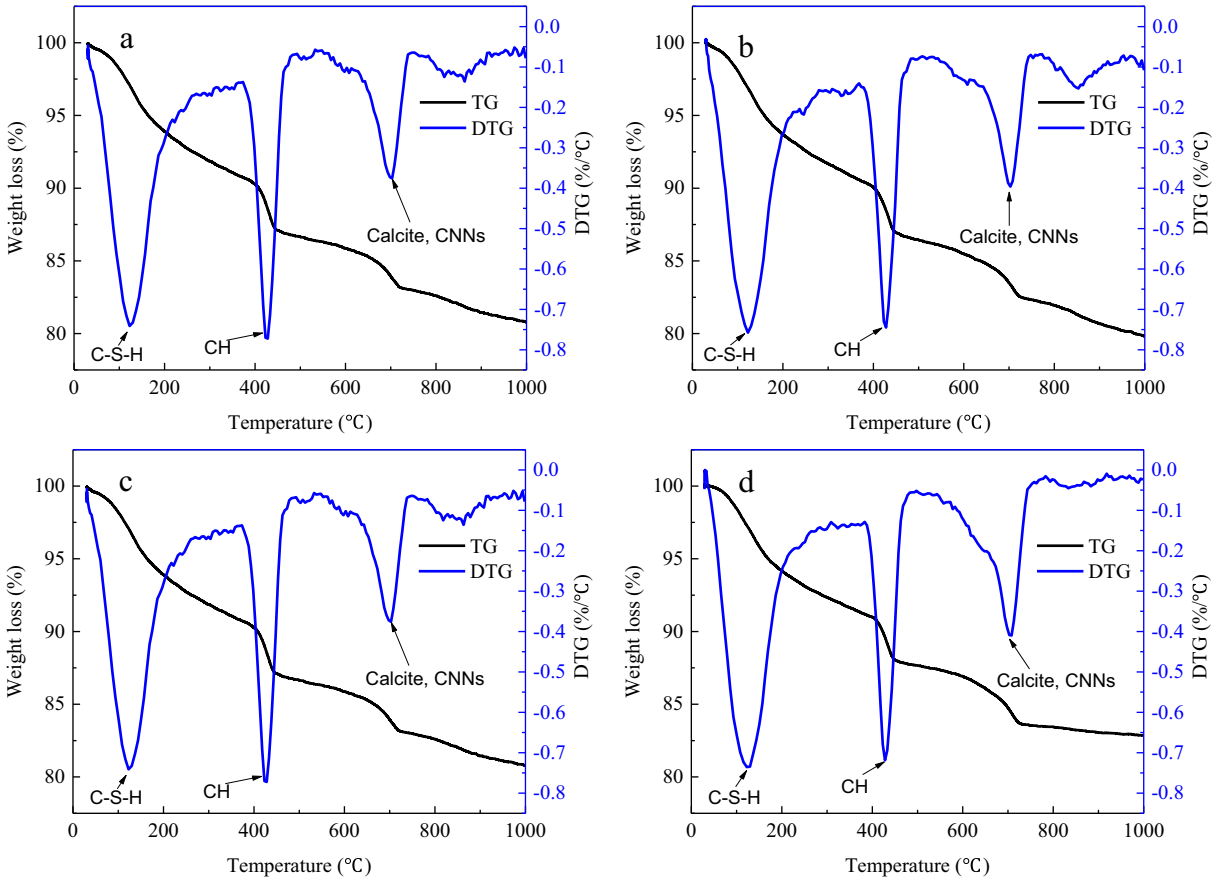

Fig. 11. TG/DTG curve of the cementitious composites with different content of CNNs: (a) 0%, (b) 0.5%, (c) 1% and (d) 2% CNNs.

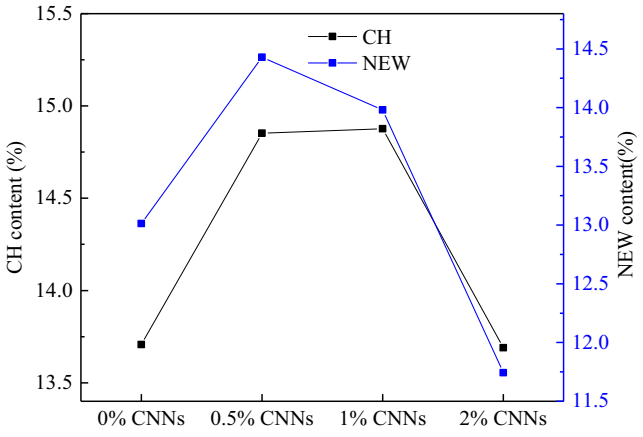

Fig. 12. CH and NEW content of cementitious composites with different content of CNNs.

$W_{1000°C}$ is the percentage of weight loss after 1000 °C heat treatment; W_{CaCO3} and W_{CNNs} are the percentage weight loss of sample after the decomposition of $CaCO_3$ and CNNs, respectively. It can be seen in Fig. 12 that the addition of 0.5 and 1% CNNs increases the NEW of cementitious composites. Especially, the NEW of 0.5% CNNs-added cement composite is 10.8% higher than that of cementitious composites without CNNs. With further increase of the CNNs dosage (2%), the NEW of cementitious composites decreases significantly. It can be deduced that a moderate amount of CNNs increases the degree of cement hydration due to the nucleation effect of CNNs, while too much CNNs impedes the polymerization of silicate chain resulting in a decreased hydration degree. The results from above hydration heat also support this observation. The weight loss between 400 °C and 500 °C is considered to be the decomposition of CH [51]. As shown in Fig. 12, with the addition of CNNs, a parabolic growth tendency of the content of CH can be observed. The content of CH in 0.5 and 1% CNNs-added cementitious composites is larger than that in other cementitious composites. This indicates that a moderate amount of CNNs can facilitates the generation of CH in cementitious composites, which is in good agreement with the deduction from the FTIR analysis.

To further explore the effects of CNNs on cement hydration, the morphology of hydration products in the cementitious composites with different CNNs dosages hydrated for 7 days was investigated by the FESEM technique. Fig. 13 shows the FESEM images of the microstructure of cementitious composites with CNNs. Noticeable changes in the micro-morphology of the composite were observed with the increase of CNNs dosage. For the plain cement composite, many immature cluster hydration products emerge in fracture surface, and some morphological needle-like hydration products disorderly stack with loose and porous structure (Fig. 13 (a)). For 0.5% and 1% addition of CNNs ((Fig. 13(b) and (c)), the characteristic immature cluster and needle-like hydrates are scarcely seen while the mature and compacted hydration products are uniformly distributed in the fracture surface, indicating higher hydration degrees compared to the plain cement paste. Those are consistent with the hydration degrees of CNNs-added cementitious composites inferred from the NEW. The most of CNNs embedded in the cementitious composites cannot be observed clearly due to the envelopment of dense hydration products. Moreover, the presence of CNNs may provide good mechanical interlocking between hydration products, which contributes to the increased hardness of the cementitious composites. These results also confirmed the conclusion aforesaid that intermixing with CNNs help improve the microscopic hardness of the cementitious composites. However, compared to the 1% CNNs-added sample, the microstructure of 2% CNNs-added cementitious composites presents more pores (Fig. 13(d), which is attributed to that the excessive CNNs would reduce the cement hydration degree and increase the probability of bleeding. This can also be responsible for the decline in microscopic hardness.

3.3. Visible light photocatalytic performance of the cementitious composites with CNNs

3.3.1. Visible light photocatalytic removal of NO_x

Cementitious composites intermixed with CNNs were employed for photocatalytic removal of NO_x in air under visible-light irradiation in a continuous mode to demonstrate their potential capability for air purification. Fig. 14 shows the photocatalytic NO_x removal performances of cementitious composites prepared with CNNs as well as 2% TiO_2 under visible-light irradiation. As can be seen, the presence of CNNs significantly enhanced the photocatalytic performance of cementitious composites. Compared to TiO_2, CNNs has a narrower band gap that can be excited directly by visible light. The removal of NO_x can be attributed to the reaction between NO_x and photogenerated radicals, producing a final product of NO_3^- [52,53]. Only an increase of 51.6% in NO_x removal efficiency was observed for the samples with 1% CNNs, compared to the samples with 0.5% CNNs (83.5 μmol m^{-2} h^{-1}). This is because most of CNNs are enveloped by the denser hydration products in the 0.5 and 1% CNNs-added cementitious composites (Fig. 13(b) and (c)), and thus they are inaccessible to the reactants or the irradiation. However, the samples with 2% CNNs acquire a NO_x removal efficiency of 227.3 μmol m^{-2} h^{-1}, which is 1.8 times higher than that of samples with 1% (126.6 μmol m^{-2} h^{-1}). This larger increase in NO_x removal efficiency is attributed to not only the higher probability of CNNs in the surface of cementitious composites, but also the more porous structure for gas diffusion and light transmittance, which is consistent with the porous morphology observed in the FESEM images (Fig. 13(d)).

3.3.2. Self-cleaning performance

The self-cleaning surface, which is one of the most appealing properties of photocatalytic building materials, can maintain their esthetic appearance over time. The removal efficiency of rhodamine B (RhB) applied on the CNNs-added cementitious composites as well as the one containing 2% TiO_2 under visible light irradiation is presented in Fig. 15. The discoloration function of the CNNs in the cementitious composites under visible light irradiation was observed clearly. The comparison of the pictures (Fig. 16) taken before and after the irradiation experiments illustrates the self-cleaning effect more explicitly. It can be found that approximately 92% of color fading occurs after 40 min exposure for 2% CNNs sample while 40% of RhB bleach for the 2% TiO_2-added cement composite in the same period. The result indicated that compared with the TiO_2-added cementitious composites, the CNNs-added ones gave a much better self-cleaning performance under visible light irradiation. However, the discoloration rate of the 0.5% CNNs sample was much lower than that of the 2% CNNs sample. It seemed that only part of the dyes that was near to the active sites of CNNs could be completely discolored leading to a much slower discoloration ratio. This is consistent with the finding shown in Fig. 13(b) that many CNNs are enveloped by compacted hydration products in the cementitious composites. With an increasing percentage of CNNs, the more porous structure (Fig. 13(d)) can promote the percolation of the dye, resulting in a higher probability of contact of dye with CNNs. This could also contribute to the discoloration. It was also found that the color of the RhB applied on the control sample (without CNNs) faded to a certain extent, which was probably due to the direct photolysis or thermolysis of the dye [54].

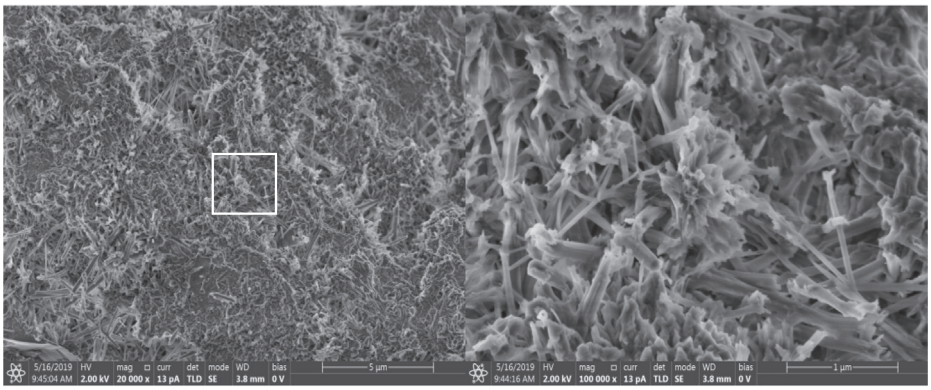

(a) 0% CNNs

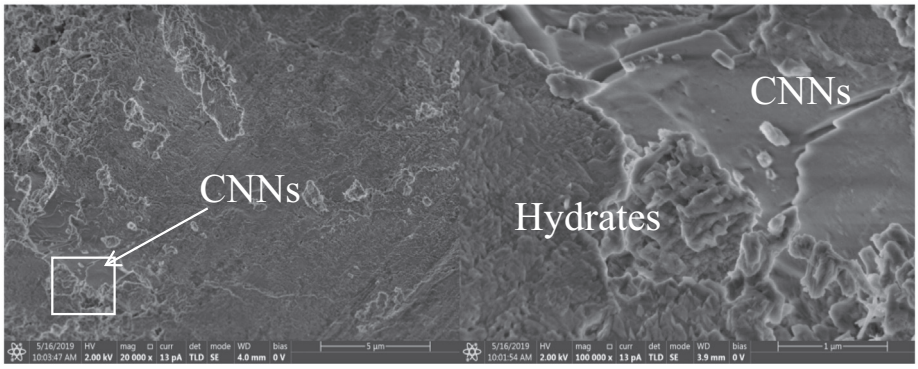

(b) 0.5% CNNs

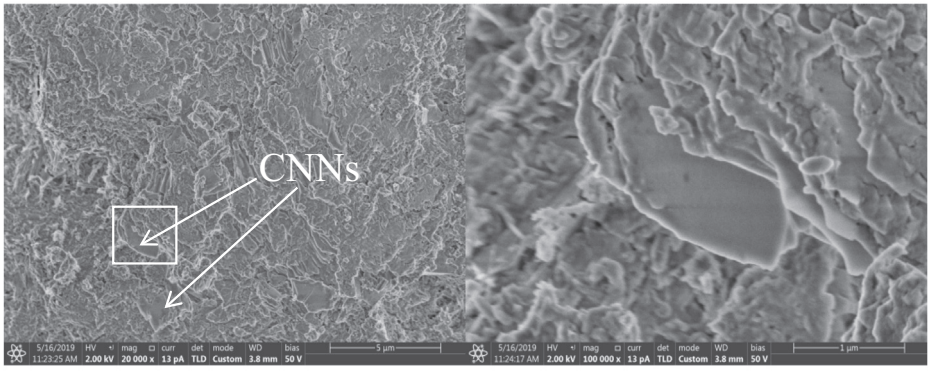

(c) 1% CNNs

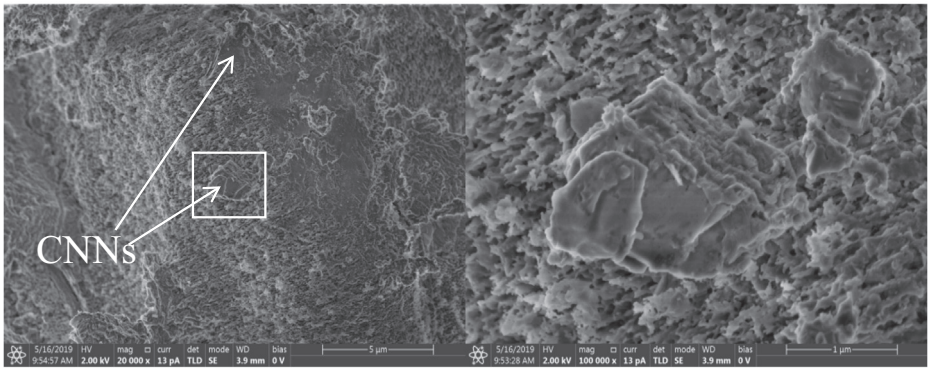

(d) 2% CNNs

Fig. 13. FESEM images of the microstructure of the cementitious composites with different content of CNNs.

According to the foregoing results, compared with the one containing TiO_2, the photocatalytic cementitious composites incorporated with CNNs exhibited a much better visible light photocatalytic activity due to the suitable band gap. With the increase of CNNs content, the photocatalytic NO_x abatement and self-cleaning performance of the photocatalytic cement composite

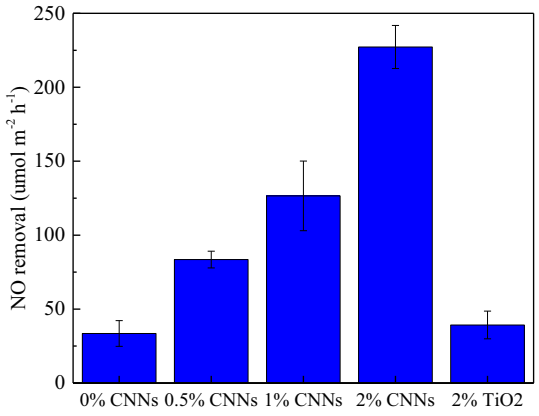

Fig. 14. The visible-light photocatalytic NO_x removal of cementitious composites with CNNs and TiO_2.

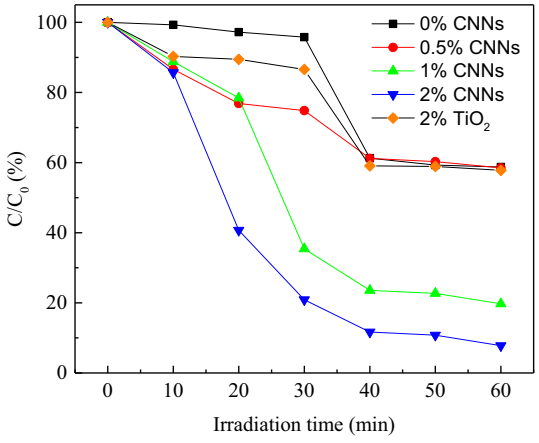

Fig. 15. The removal efficiency of RhB applied on the cementitious composites with CNNs and TiO_2 under the irradiation of visible light.

increased. For the 2% CNNs-added cementitious composites, excessive CNNs decreased the degree of cement hydration, but the microscopic hardness was 5.4% higher than that of the control due to the strengthen effect of CNNs. Moreover, among all the samples, the one with 2% CNNs showed the highest photocatalytic NO_x abatement efficiency of 227.3 μmol m^{-2} h^{-1}, and degraded the RhB within 40 min.

4. Conclusions

The work reported in this paper aims to promote the practical environmental application of an earth-abundant g-C_3N_4 photocatalyst in cementitious composites. The main conclusions are listed below.

(1) With the increase of CNNs content, the hydration degree and micro-hardness increase first and then decrease. The microscopic hardness of 0.5% CNNs-added cement composite shows an improvement of 18% compared with the one without CNNs. For the 2% CNNs-added cement composite, excessive CNNs decreases the degree of cement hydration, but the microscopic hardness is still 5.4% higher than that of the control due to the strengthen effect of CNNs.
(2) As the growth points for hydration products, the CNNs gave a strong bond with hydration products, which improved the load-transfer efficiency from the cementitious composites to CNNs.
(3) With the increase of CNNs content, the photocatalytic NO_x abatement and self-cleaning performance of the photocatalytic cementitious composites increased. Among all the cementitious composites that were tested, the one with 2% CNNs showed the highest photocatalytic NO_x abatement efficiency of 227.3 μmol m^{-2} h^{-1}, and degraded the rhodamine B within 40 min. Compared with the TiO_2 based cementitious composites, the one incorporated with CNNs gave a much better visible light photocatalytic activity due to the suitable band gap. It was found that a moderate amount of CNNs (below 2%) CNNs could be used in cementitious composites for the photocatalytic depollution

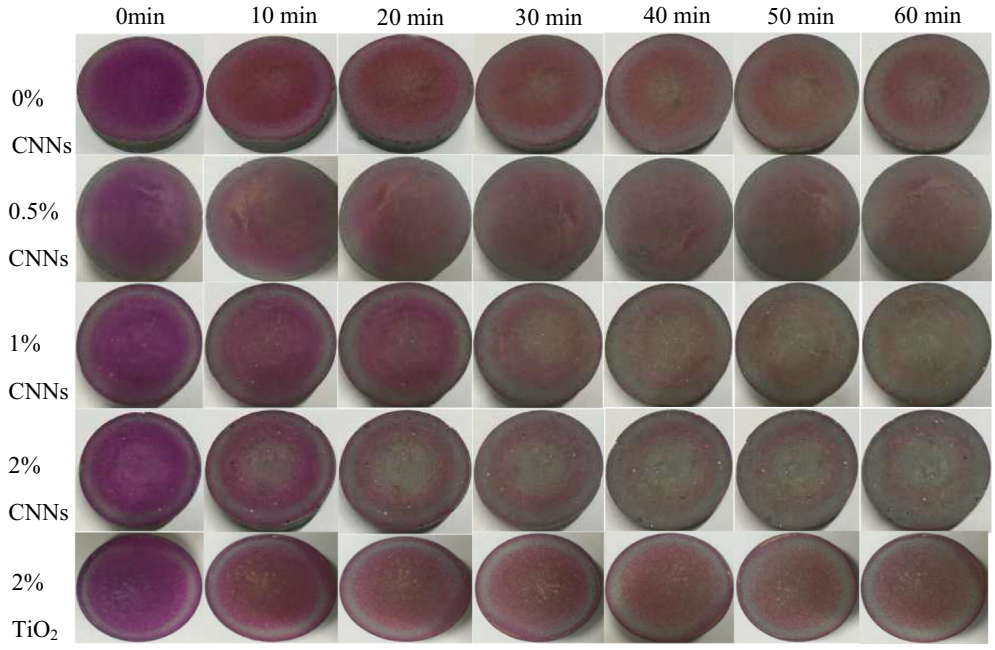

Fig. 16. Color variation of RhB coated on cementitious composites with CNNs and TiO_2.

performance without adverse effect on mechanical properties of the cementitious composites. This work is expected to help broaden the application of photocatalytic cementitious materials in sustainable building and constructions for improved environmental pollution mitigation.

Declaration of Competing Interest

The authors declare that there is no conflict of interest regarding the publication of this article.

Acknowledgements

This work was supported by "Minjiang Scholar" program of Fujian province, China (No. Min-Jiaogao [2018]-56), Natural Science Fundation of Fujian province (grant number 2019J01235), and the Center for Environmentally Sustainable Transportation in Cold Climates (CESTiCC) under project No. 1630 at Washington State University – United States.

References

[1] F. Rodriguez-Rivas, A. Pastor, C. Barriga, M. Cruz-Yusta, L. Sánchez, I. Pavlovic, Zn-Al layered double hydroxides as efficient photocatalysts for NO_x abatement, Chem. Eng. J. 346 (2018) 151–158.
[2] A. Trapalis, N. Todorova, T. Giannakopoulou, N. Boukos, T. Speliotis, D. Dimotikali, J. Yu, TiO_2/graphene composite photocatalysts for NO_x removal: a comparison of surfactant-stabilized graphene and reduced graphene oxide, Appl. Catal., B 180 (2016) 637–647.
[3] M. Pérez-Nicolás, I. Navarro-Blasco, J.M. Fernández, J.I. Alvarez, Atmospheric NO_x removal: study of cement mortars with iron-and vanadium-doped TiO_2 as visible light–sensitive photocatalysts, Constr. Build. Mater. 149 (2017) 257–271.
[4] J. Ângelo, L. Andrade, L.M. Madeira, A. Mendes, An overview of photocatalysis phenomena applied to NO_x abatement, J. Environ. Manage. 129 (2013) 522–539.
[5] M. Pérez-Nicolás, J. Balbuena, M. Cruz-Yusta, L. Sánchez, I. Navarro-Blasco, J. Fernández, J. Alvarez, Photocatalytic NO_x abatement by calcium aluminate cements modified with TiO_2: Improved NO_2 conversion, Cem. Concr. Res. 70 (2015) 67–76.
[6] A. Aziz, K.S. Kim, Synergistic effect of UV pretreated Fe-ZSM-5 catalysts for heterogeneous catalytic complete oxidation of VOC: a technology development for sustainable use, J. Hazard. Mater. 340 (2017) 351–359.
[7] M.-Z. Guo, T.-C. Ling, C.-S. Poon, Nano-TiO_2-based architectural mortar for NO removal and bacteria inactivation: Influence of coating and weathering conditions, Cem. Concr. Compos. 36 (2013) 101–108.
[8] M.V. Diamanti, R. Paolini, M. Rossini, A.B. Aslan, M. Zinzi, T. Poli, M.P. Pedeferri, Long term self-cleaning and photocatalytic performance of anatase added mortars exposed to the urban environment, Constr. Build. Mater. 96 (2015) 270–278.
[9] T. Martinez, A. Bertron, E. Ringot, G. Escadeillas, Degradation of NO using photocatalytic coatings applied to different substrates, Build. Environ. 46 (9) (2011) 1808–1816.
[10] J. Ângelo, L. Andrade, A. Mendes, Highly active photocatalytic paint for NO_x abatement under real-outdoor conditions, Appl. Catal., A 484 (2014) 17–25.
[11] M.-Z. Guo, C.-S. Poon, Photocatalytic NO removal of concrete surface layers intermixed with TiO_2, Build. Environ. 70 (2013) 102–109.
[12] A.M. Ramirez, K. Demeestere, N. De Belie, T. Mäntylä, E. Levänen, Titanium dioxide coated cementitious materials for air purifying purposes: preparation, characterization and toluene removal potential, Build. Environ. 45 (4) (2010) 832–838.
[13] A. Calia, M. Lettieri, M. Masieri, S. Pal, A. Licciulli, V. Arima, Limestones coated with photocatalytic TiO_2 to enhance building surface with self-cleaning and depolluting abilities, J. Cleaner Prod. 165 (2017) 1036–1047.
[14] T. Vulic, O. Rudic, S. Vucetic, D. Lazar, J. Ranogajec, Photocatalytic activity and stability of TiO_2/ZnAl layered double hydroxide based coatings on mortar substrates, Cem. Concr. Compos. 58 (2015) 50–58.
[15] D. Macphee, A. Folli, Photocatalytic concretes—The interface between photocatalysis and cement chemistry, Cem. Concr. Res. 85 (2016) 48–54.
[16] X. Wang, K. Maeda, A. Thomas, K. Takanabe, G. Xin, J.M. Carlsson, K. Domen, M. Antonietti, A metal-free polymeric photocatalyst for hydrogen production from water under visible light, Nat. Mater. 8 (1) (2009) 76–80.
[17] D.J. Martin, K. Qiu, S.A. Shevlin, A.D. Handoko, X. Chen, Z. Guo, J. Tang, Highly efficient photocatalytic H_2 evolution from water using visible light and structure-controlled graphitic carbon nitride, Angew. Chem. Int. Ed. 53 (35) (2014) 9240–9245.
[18] R. Kuriki, K. Sekizawa, O. Ishitani, K. Maeda, Visible-light-driven CO_2 reduction with carbon nitride: enhancing the activity of ruthenium catalysts, Angew. Chem. Int. Ed. 54 (8) (2015) 2406–2409.
[19] G. Mamba, A. Mishra, Graphitic carbon nitride (g-C_3N_4) nanocomposites: a new and exciting generation of visible light driven photocatalysts for environmental pollution remediation, Appl. Catal., B 198 (2016) 347–377.
[20] W.-J. Ong, L.-L. Tan, Y.H. Ng, S.-T. Yong, S.-P. Chai, Graphitic carbon nitride (g-C_3N_4)-based photocatalysts for artificial photosynthesis and environmental remediation: are we a step closer to achieving sustainability?, Chem Rev. 116 (12) (2016) 7159–7329.
[21] F. Chang, C. Li, J. Luo, Y. Xie, B. Deng, X. Hu, Enhanced visible-light-driven photocatalytic performance of porous graphitic carbon nitride, Appl. Surf. Sci. 358 (2015) 270–277.
[22] I. Papailias, T. Giannakopoulou, N. Todorova, D. Demotikali, T. Vaimakis, C. Trapalis, Effect of processing temperature on structure and photocatalytic properties of g-C_3N_4, Appl. Surf. Sci. 358 (2015) 278–286.
[23] T. Sano, S. Tsutsui, K. Koike, T. Hirakawa, Y. Teramoto, N. Negishi, K. Takeuchi, Activation of graphitic carbon nitride (g-C_3N_4) by alkaline hydrothermal treatment for photocatalytic NO oxidation in gas phase, J. Mater. Chem. A 1 (21) (2013) 6489–6496.
[24] P. Niu, L. Zhang, G. Liu, H.M. Cheng, Graphene-like carbon nitride nanosheets for improved photocatalytic activities, Adv. Funct. Mater. 22 (22) (2012) 4763–4770.
[25] K. Schwinghammer, M.B. Mesch, V. Duppel, C. Ziegler, J.r. Senker, B.V. Lotsch, Crystalline carbon nitride nanosheets for improved visible-light hydrogen evolution, J. Am. Chem. Soc. 136(5) (2014) 1730-1733.
[26] F. Peng, Y. Ni, Q. Zhou, J. Kou, C. Lu, Z. Xu, New g-C_3N_4 based photocatalytic cement with enhanced visible-light photocatalytic activity by constructing muscovite sheet/SnO_2 structures, Constr. Build. Mater. 179 (2018) 315–325.
[27] X. Lu, K. Xu, P. Chen, K. Jia, S. Liu, C. Wu, Facile one step method realizing scalable production of g-C_3N_4 nanosheets and study of their photocatalytic H_2 evolution activity, J. Mater. Chem. A 2 (44) (2014) 18924–18928.
[28] D.F. Aponte, M. Barra, E. Vàzquez, Durability and cementing efficiency of fly ash in concretes, Constr. Build. Mater. 30 (2012) 537–546.
[29] I.F. Olmo, E. Chacon, A. Irabien, Influence of lead, zinc, iron (III) and chromium (III) oxides on the setting time and strength development of Portland cement, Cem. Concr. Res. 31 (8) (2001) 1213–1219.
[30] G. Bernardo, A. Telesca, G.L. Valenti, A porosimetric study of calcium sulfoaluminate cement pastes cured at early ages, Cem. Concr. Res. 36 (6) (2006) 1042–1047.
[31] R.A. Cook, K.C. Hover, Mercury porosimetry of hardened cement pastes, Cem. Concr. Res. 29 (6) (1999) 933–943.
[32] B. Das, P.K. Eswar, U. Ramamurty, C.N. Rao, Nano-indentation studies on polymer matrix composites reinforced by few-layer graphene, Nanotechnology 20 (12) (2009) 125705.
[33] P. Hou, S. Kawashima, D. Kong, D.J. Corr, J. Qian, S.P. Shah, Modification effects of colloidal nanoSiO_2 on cement hydration and its gel property, Composites Part B 45 (1) (2013) 440–448.
[34] M.-Z. Guo, C.S. Poon, Superior photocatalytic NO_x removal of cementitious materials prepared with white cement over ordinary Portland cement and the underlying mechanisms, Cem. Concr. Compos. 90 (2018) 42–49.
[35] J. Chen, S.-C. Kou, C.-S. Poon, Photocatalytic cement-based materials: Comparison of nitrogen oxides and toluene removal potentials and evaluation of self-cleaning performance, Build. Environ. 46 (9) (2011) 1827–1833.
[36] H. Du, S. Dai Pang, Dispersion and stability of graphene nanoplatelet in water and its influence on cement composites, Constr. Build. Mater. 167 (2018) 403–413.
[37] Z. Wu, C. Shi, K.H. Khayat, S. Wan, Effects of different nanomaterials on hardening and performance of ultra-high strength concrete (UHSC), Cem. Concr. Compos. 70 (2016) 24–34.
[38] K.L. Scrivener, A. Nonat, Hydration of cementitious materials, present and future, Cem. Concr. Res. 41 (7) (2011) 651–665.
[39] C. Hesse, F. Goetz-Neunhoeffer, J. Neubauer, A new approach in quantitative in-situ XRD of cement pastes: Correlation of heat flow curves with early hydration reactions, Cem. Concr. Res. 41 (1) (2011) 123–128.
[40] D. Jansen, F. Goetz-Neunhoeffer, B. Lothenbach, J. Neubauer, The early hydration of Ordinary Portland Cement (OPC): An approach comparing measured heat flow with calculated heat flow from QXRD, Cem. Concr. Res. 42 (1) (2012) 134–138.
[41] V.V. Rocha, P. Ludvig, A.C.C. Trindade, F. de Andrade Silva, The influence of carbon nanotubes on the fracture energy, flexural and tensile behavior of cement based composites, Constr. Build. Mater. 209 (2019) 1–8.
[42] N.H. de Azevedo, P.J. Gleize, Effect of silicon carbide nanowhiskers on hydration and mechanical properties of a Portland cement paste, Constr. Build. Mater. 169 (2018) 388–395.
[43] B. Han, Q. Zheng, S. Sun, S. Dong, L. Zhang, X. Yu, J. Ou, Enhancing mechanisms of multi-layer graphenes to cementitious composites, Composites Part A 101 (2017) 143–150.
[44] Y. Qing, Z. Zenan, K. Deyu, C. Rongshen, Influence of nano-SiO_2 addition on properties of hardened cement paste as compared with silica fume, Constr. Build. Mater. 21 (3) (2007) 539–545.
[45] R. Ylmén, U. Jäglid, B.-M. Steenari, I. Panas, Early hydration and setting of Portland cement monitored by IR, SEM and Vicat techniques, Cem. Concr. Res. 39 (5) (2009) 433–439.

[46] S.A.E. Aleem, M. Heikal, W. Morsi, Hydration characteristic, thermal expansion and microstructure of cement containing nano-silica, Constr. Build. Mater. 59 (2014) 151–160.
[47] M. Wu, Y. Zhang, Y. Jia, W. She, G. Liu, Z. Wu, W. Sun, Influence of sodium hydroxide on the performance and hydration of lime-based low carbon cementitious materials, Constr. Build. Mater. 200 (2019) 604–615.
[48] M.S. Kim, Y. Jun, C. Lee, J.E. Oh, Use of CaO as an activator for producing a price-competitive non-cement structural binder using ground granulated blast furnace slag, Cem. Concr. Res. 54 (2013) 208–214.
[49] I. Galan, L. Perron, F.P. Glasser, Impact of chloride-rich environments on cement paste mineralogy, Cem. Concr. Res. 68 (2015) 174–183.
[50] M.S. Lemos, A.L.C.D. Cunha, J. Dweck, A study of cement Type II hydration partially substituted by Brazilian spent cracking catalyst fines, J. Therm. Anal. Calorim. 130 (1) (2017) 573–584.
[51] S. Cui, P. Liu, J. Su, E. Cui, C. Guo, B. Zhu, Experimental study on mechanical and microstructural properties of cement-based paste for shotcrete use in high-temperature geothermal environment, Constr. Build. Mater. 174 (2018) 603–612.
[52] X. Li, D. Chen, N. Li, Q. Xu, H. Li, J. He, J. Lu, One-step synthesis of honeycomb-like carbon nitride isotype heterojunction as low-cost, high-performance photocatalyst for removal of NO, ACS Sustainable Chem. Eng. 6 (8) (2018) 11063–11070.
[53] J. Hu, D. Chen, N. Li, Q. Xu, H. Li, J. He, J. Lu, Fabrication of graphitic-C_3N_4 quantum dots/graphene-$InVO_4$ aerogel hybrids with enhanced photocatalytic NO removal under visible-light irradiation, Appl. Catal., B 236 (2018) 45–52.
[54] B. Ruot, A. Plassais, F. Olive, L. Guillot, L. Bonafous, TiO_2-containing cement pastes and mortars: measurements of the photocatalytic efficiency using a rhodamine B-based colourimetric test, Sol. Energy 83 (10) (2009) 1794–1801.